Analytical Potential Energy Surface Describing Abstraction Reactions in Asymmetrically substituted Polyatomic Systems of Type $CX_3Y + A \rightarrow$ Products†

Cipriano Rangel and Joaquín Espinosa-García*

Departamento de Química Física, Universidad de Extremadura, 06071 Badajoz, Spain

Received: May 3, 2005; In Final Form: July 7, 2005

The gas-phase reaction between chloromethane and hydrogen proceeds by two channels, Cl- and H-abstraction, and was chosen as a model of asymmetrically substituted polyatomic reactions of type $CX_3Y + A \rightarrow$ products. The analytical potential energy surface for this reaction was constructed with suitable functional forms to represent vibrational modes, and both channels were independently fitted to reproduce experimental and theoretical information only at the stationary points. The rate constants for the Cl- and H-channels and the overall reaction were calculated using variational transition-state theory with multidimensional tunneling effect over a wide temperature range, 298−3000 K. The Cl-abstraction reaction is preferred until 2100 K, while above this temperature the H-abstraction channel is favored. The theoretical overall rate constants agree with the experimental data in the common temperature range, 500−800 K, with a small curvature of the Arrhenius plot due mainly to the role of the tunneling in the H-abstraction channel. This surface was then used to analyze dynamical features, such as reaction-path curvature, and coupling between the reaction-coordinate and vibrational modes. It was found qualitatively that excitation of the C−Cl and C−H stretching reactive modes enhances the forward rate constants for the Cl- and H-abstraction channels, respectively, and only the Cl−H and H−H stretching modes in the products of the Cl- and H-abstraction reactions, respectively, appear vibrationally excited.

I. Introduction

The construction of potential energy surfaces (PES) for polyatomic systems represents a field of growing interest in molecular kinetics and dynamics. Actually, the exponential increase of computational power permits the calculation of thousands of geometrical configurations, which can be interpolated or fitted to a suitable functional form, to obtain the PES. This alternative gives adequate PESs only when ab initio calculations of very high-level are used, which is still today prohibitive for atoms beyond the second-row, and usually requires a posteriori a final refit.

An alternative to this very expensive process is to choose a suitable functional form, which correctly describes the stretching and bending movements of the system, and calibrate it against theoretical and/or experimental information. Clearly, in this sense, the surface is semiempirical. This economic alternative has been extensively used by our group in several reactions,[1−8] and it represents a very useful and less time-consuming alternative. Until now we had applied this strategy to symmetrically substituted polyatomic reactions of type $CX_4 + A$, where all the X atoms are equivalent and A is the abstractor atom. This equivalent character of the four bonds C−X and angles X−C−X allowed a simplification of the problem, because all bonds and angles were treated in the same way. Now, in this paper, we propose an extension of this method to asymmetrically substituted polyatomic reactions, CWXYZ + A, and we begin by analyzing a simple case with two different substituents, $CX_3Y + A$. Clearly, this represents a complication in the PES construction because now the bonds and angles must be independently treated, but it makes it possible to study different pathways.

To test this new strategy, we shall build the PES for the CH_3-Cl + H abstraction reaction, which can proceed through two channels, chlorine and hydrogen abstractions:

$$CH_3Cl + H \rightarrow CH_3 + ClH \quad (R1)$$

$$\rightarrow CH_2Cl + H_2 \quad (R2)$$

This reaction presents several important features that invite theoretical study. First, the study of chlorinated hydrocarbons (CHCs) is of great importance in atmospheric and combustion processes. Second, the experimental rate constants[9−14] show a broad range of values, with differences of 1 order of magnitude, although the recent critical revision performed by Bryukov et al.[14] gives support to their results, which coincide with the previous measurements by Westenberg and deHass.[10] Third, with respect to the branching ratio, $\tau_X = k_X/(k_1 + k_2)$, where X refers to the X-abstraction pathway and k_Xs are the respective rate constants for each channel, the situation is more disappointing. No experimental information is available on this ratio, and the theoretical results[14−17] are contradictory. Thus, Knyazev[15] and Sheng et al.[16] found that the H-abstraction channel, R2, is the more important, while Bryukov et al.[14] and Louis et al.[17] found that the predominant channel is the Cl-abstraction, R1. Finally, another important feature is that this reaction can proceed through two pathways, which would multiply the computational effort needed to describe both surfaces if interpolation or fitting procedures are used. In this case, the strategy of functional form plus calibration presented in this paper is even more advantageous.

The paper is organized as follows. In section II, high-level electronic structure calculations are performed to estimate the

† Part of the special issue "Donald G. Truhlar Festschrift".

* Corresponding author. E-mail: joaquin@unex.es.

10.1021/jp052297z CCC: $33.50
Published on Web 08/09/2005

TABLE 1: Saddle Point Energy Calculations Using Several Levels

	Cl-channel		H-channel	
method	$\Delta E^{\ddagger}$	$\Delta H^{\ddagger}$(0 K)	$\Delta E^{\ddagger}$	$\Delta H^{\ddagger}$(0 K)
K[a]	10.7	10.8	13.4	11.8
SLLXS[b]	10.7	10.4	12.8	11.1
LGS[c]	9.7	9.6	12.5	11.2
this work[d]	11.3	10.9	13.1	11.4
this work[e]	9.3	8.9	12.6	10.8

[a] Reference 15. Single-point calculation QCISD(T)/6-311+G(2d,2p)//MP2/6-311G(2d,2p). [b] Reference 16. Single-point calculation PMP4//BH&HLYP/6-311+G(3df,2p). [c] Reference 17. Single-point calculation CCSD(T)/6-311++G(3df,3pd)//UMP2/6-311++G(d,p). [d] Single-point calculation CCSD(T)/cc-pVTZ//CCSD(T)/6-31G(d,p). [e] Extrapolated to infinite basis using the IB method.[18,19]

SCHEME 1

PES-permutation	Substituent	Type
Symmetric	Equivalent	CX_4+A
Symmetric	Non-equivalent	CX_3Y+A

barrier heights of the Cl- and H-abstraction channels, R1 and R2, respectively, which are sensitive parameters in the calibration process. In section III, first the new PES is constructed and calibrated, and second, it is tested against experimental and theoretical values. The results are given in section IV, and section V presents the conclusions.

II. Electronic Structure Calculations. Estimation of the Barrier Heights

It is well-known that the classical barrier height is very sensitive to extension of the one-electron basis set, and that truncation of the one-electron basis set is the major source of error in most ab initio calculations of molecular energies. In this work, to obtain the basis set limit, we use Truhlar's infinite basis-set extrapolation method (IB)[18,19] based on the CCSD(T) level with cc-pVDZ and cc-pVTZ basis sets (correlation-consistent polarized valence double- and triple-ζ).[20] This method yields more accurate energies than those from straight correlation consistent polarized sextuple-ζ at < 1% of the cost.[18,19] The total energy for the IB method is

$$E_{\infty}^{Total} = E_{\infty}^{HF} + E_{\infty}^{corr}$$

$$E_{\infty}^{Total} = \frac{3^{\alpha}}{3^{\alpha}-2^{\alpha}}E_3^{HF} - \frac{2^{\alpha}}{3^{\alpha}-2^{\alpha}}E_2^{HF} + \frac{3^{\beta}}{3^{\beta}-2^{\beta}}E_3^{corr} - \frac{2^{\beta}}{3^{\beta}-2^{\beta}}E_2^{corr} \quad (1)$$

where "*corr*" is the correlation energy, "*HF*" is the Hartree−Fock energy, and the subscripts 2 and 3 represent the energies using the double- or triple-ζ basis, respectively. The parameters α and β have values 3.39 and 2.02, respectively.

Table 1 gives the IB barrier heights for the two channels (Cl- and H-abstractions), together with other theoretical values for comparison. While our barrier heights at the unextrapolated CCSD(T)/cc-pVTZ level are 11.3 and 13.1 kcal mol^{-1} for the Cl- and H-abstraction, respectively, in agreement with the previous and unextrapolated theoretical results,[14−17] using the extrapolated Scheme 1B, lower barriers are obtained, 9.3 and 12.6 kcal mol^{-1}, respectively, in agreement with very recent calculations by Louis et al.,[17] by using high-level calculations with polarization and diffuse functions. When the zero-point energy (ZPE) is included, the conventional transition-state enthalpy of activation at 0 K, $\Delta H^{\ddagger}_{o}$, is obtained, with values of 8.9 and 10.8 kcal mol^{-1}, respectively. These will be the values used to fit the new potential energy surface (section III.2).

III. Potential Energy Surface

1. Functional Form. On the basis of our previous experience with symmetrically substituted polyatomic reaction of type CX_4 + A, the new surface for the asymmetrically substituted reaction of type CX_3Y + A is formulated in similar terms, i.e., stretching (str), valence (val) bending, and out-of-plane (op) bending, and has the general form

$$V = V_{str} + V_{op} + V_{val} \quad (2)$$

where V_{str} is the stretching term given by

$$V_{str} = \sum_{i=1}^{3}[V_3(R_{CH_i}',R_{CHa},R_{H'Ha})] + V_3(R_{CCl},R_{CHa},R_{ClHa}) \quad (3)$$

where H_a and H′ are the abstractor and abstracted hydrogens, respectively, and V_3 represents the London−Eyring−Polanyi (LEP) functional form. Each V_3 term involves a singlet curve depending on three parameters ($^1D_{U-V}$, α_{U-V}, and R°_{U-V}) and a triplet curve depending on five parameters ($^3D_{U-V}$, β_{U-V}, c_{U-V}, a_{U-V}, and R°_{U-V}) for each U−V bond. Note that unlike our previous reaction of type CX_4 + A, in this case we have separated the V_3 terms between the three equivalent hydrogens and the chlorine atom. The C−H and C−Cl Morse parameters, α_{C-H} and α_{C-Cl} are allowed to relax using a switching function, from reactant, CH_3Cl, to radical products, CH_3 or CH_2Cl, depending on the pathway chosen

$$\alpha_{U-V} = a_{U-V} + b_{U-V}\left(\frac{\tanh[c_{U-V}(R-R^{o})]+1}{2}\right) \quad (4)$$

where R is the C−Cl bond length or the average of the three shortest C−H bond lengths in the system, R° is the equilibrium C−H or C−Cl bond lengths in the reactant, CH_3Cl, and a_{U-V}, b_{U-V}, and c_{U-V} are adjustable parameters to obtain accurate stretching frequencies at the CH_3Cl ($R = R^{\circ}$), at the products, CH_3 or CH_2Cl ($R = \infty$), and at the saddle point. This separation of the C−Cl and C−H stretching modes permits us to separate the two channels, Cl- and H-abstraction, using the same functional form.

V_{val} is a harmonic term for valence bending

$$V_{val} = \frac{1}{2}\sum_{i=1}^{2}\sum_{j=i+1}^{3}k_o k_i k_j(\theta_{ij}-\theta_{ij}^{o})^2 + \frac{1}{2}\sum_{i=1}^{3}k_o' k_i' k_l(\theta_{il}-\theta_{il}^{o})^2 \quad (5)$$

where the first sum is over the three H−C−H angles involving two methyl H's, and the second sum is over the three H−C−Cl angles. The force constants, k, are adjustable parameters, and the reference angles θ_{ij}° and θ_{il}° represent the equilibrium angles defined by the *i*th and *j*th C−H bonds, and the *i*th C−H bond and C−Cl bond, respectively, in the halomethane, and are also allowed to relax using a switching function from the halomethane to CH_3 or CH_2Cl radicals depending on the pathway chosen. As in the case of the V_{str} term, we have separated the V_{val} terms between the H−C−H and H−C−Cl angles.

Finally, V_{op} is the bending out-of-plane term, correlating with the out-of-plane motion of the product radical, CH_3 or CH_2Cl, depending on the pathway chosen. Again, we separated the

TABLE 2: Geometrical Parameters[a] of Reactants and Products

species	geometrical parameters	PES−Cl	PES−H	expt[b]	theor			
CH_3Cl	r_{C-Cl}	1.760	1.760	1.781				
	r_{C-H}	1.094	1.094	1.096				
	$\angle_{Cl-C-H}$	109.5	109.5	110.5				
	$\angle_{H-C-H}$	109.5	109.5	108.0				
	frequency	3249 (e)[c]	3215 (e)[c]	3054 (e)				
		3221	3196	2968				
		1516 (e)	1543 (e)	1455 (e)				
		1322	1355	1355				
		862 (e)	916 (e)	1017 (e)				
		728	708	732				
CH_3	r_{C-H}	1.094		1.079				
	$\angle_{H-C-H}$	120.0		120.0				
	frequency	3185		3002				
		2952 (e)		3184 (e)				
		1529 (e)		1383 (e)				
		582		580				
HCl	r_{H-Cl}	1.275		1.275				
	frequency	2847		2890				
Cl-channel	energy							
	ΔH_r(0 K)	−18.3		−19.9				
CH_2Cl	r_{C-Cl}		1.760		1.697[d]	1.709[e]	1.688[f]	1.689[g]
	r_{C-H}		1.094		1.072	1.077	1.068	1.068
	$\angle_{Cl-C-H}$		120.0		118.0	117.6	117.9	117.7
	$\angle_{H-C-H}$		120.0		124.0	124.8	124.2	124.6
	dihedral angle		180.0		163.5	166.4	175.0	180.0
	frequency		3201		3448	3394	3398	3403
			3177		3294	3245	3265	3267
			1502		1506	1480	1466	1464
			914		1057	1035	1026	1026
			707		886	861	882	880
			490		334	265	199	141
H_2	r_{H-H}		0.742	0.741				
	frequency		4406	4405				
H-channel	energy							
	ΔH_r(0 K)		−4.4	−5.2				

[a] Distances in angstrom, angles in degrees, and energies in kcal mol^{-1}. [b] Reference 22. [c] We have found small differences of the vibrational frequencies for the CH_3Cl reactant by using the two parameters sets, which only represent a difference of 0.2 kcal mol^{-1} in the zero-point energy. [d] This work, at the MP2/6-31G(d,p) level (C_s symmetry). At this level the planar structure is not a true minimum. [e] This work, at the CCSD(T)/6-31G(d,p) level (C_s symmetry). At this level the planar structure is not a true minimum. [f] This work, at the MP2/cc-pVTZ level (C_s symmetry). [g] This work, at the MP2/cc-pVTZ level. Planar structure (C_{2v} symmetry).

H−C−Cl−H and H−C−H−H dihedral angles, and the expression is

$$V_{op} = \sum_{i=1}^{4} f_{\Delta i} \sum_{j=1,j\neq i}^{4} \Delta_{ij}^{\ 2} + \sum_{i=1}^{4} h_{\Delta i} \sum_{j=1,j\neq i}^{4} \Delta_{ij}^{\ 4} \qquad (6)$$

The functional form is based on symmetric terms suggested by Duchovic et al.,[21] where

$$f_{\Delta i} = ([1 - S_3(R_i)]\cdot S_3(R_j)\cdot S_3(R_k)\cdot S_3(R_l))\cdot f_{\Delta}^{CH3} \qquad (7)$$

$$h_{\Delta i} = ([1 - S_3(R_i)]\cdot S_3(R_j)\cdot S_3(R_k)\cdot S_3(R_l))\cdot h_{\Delta}^{CH3} \qquad (8)$$

$$S_3(R) = 1 - \tanh\,[\alpha_3(R - R^o)(R - \beta_3)^2] \qquad (9)$$

with R being each of the C−Hi and C−Cl bonds and $R°$ being the correspondent equilibrium value, and

$$\Delta_{ij} = \cos^{-1}\left[\frac{(r_k - r_j)\times(r_l - r_j)}{||(r_k - r_j)\times(r_l - r_j)||}\cdot\frac{r_i}{||r_i||}\right] - \phi_{ij}^{o} \qquad (10)$$

where the vectors **r** are associated with the bonds R.

In sum, in this new PES we have separated the functional forms for the three equivalent H's and the chlorine atom, and we have introduced 10 new calibration parameters, describing the behavior of the different chlorine atom. Note that as in the case of our previous PESs, this new PES is also symmetric with respect to the permutation of the equivalent methyl hydrogens, a very important feature in dynamics studies. Therefore, to clarify the nomenclature, it is necessary to note that until now we had used symmetric PESs to describe symmetrically substituted polyatomic reactions, $CX_4 + A$, and now with this work, we are introducing symmetric PESs to describe asymmetrically substituted polyatomic reactions, $CX_3Y + A$. Scheme 1 summarizes these differences.

2. Calibration Process. Having selected the functional form, the calibration of the PES is considered for each channel (chlorine and hydrogen abstraction) independently, obtaining two independent sets of parameters. This process has been described in detail elsewhere,[1−8] and we shall present here a short description of the process, although in this case, due to the existence of two channels, it has been necessary to introduce some modifications. The calibration process consists of two steps. In the first step, for each channel, we change the parameters of the PES related to the geometric, energy, and vibrational properties of the reactants and products, so that the geometries, heat of reaction, and vibrational frequencies agree with the available experimental data. In the second step, for each channel, we refit some parameters in order to reproduce the characteristics of the quantum mechanically calculated saddle point, in particular, the geometry, barrier height, and vibrational frequencies. In this case, we would note that the rate constants

TABLE 3: Geometrical Parameters[a] of the Saddle Point at Several Levels

	PES	CCSD(T)[b]	BSK[c]	K[d]	SLLXS[e]	LGS[f]
			Cl-Channel			
r_{C-Cl}	1.932	1.970	1.957	1.964	1.958	1.951
r_{C-H}	1.084	1.084	1.081	1.079	1.077	1.086
r_{Hb-Cl}	1.804	1.631	1.561	1.581	1.661	1.563
$\angle_{C-Cl-Hb}$	180.0	180.0	180.0	180.0	180.0	180.0
$\angle_{H-C-H}$	114.9	113.3		113.5	113.6	
$\angle_{Cl-C-H}$	103.2	105.3	105.4	105.1	104.9	105.5
frequency	3207	3152	3004	3139	3175	3127
	3145 (e)	3295 (e)	3150 (e)	3284 (e)	3313 (e)	3274 (e)
	1525 (e)	1501 (e)	1427 (e)	1485 (e)	1502 (e)	1462 (e)
	804	1281	1224	1255	1287	1287
	759	869 (e)	1038 (e)	861 (e)	890 (e)	874 (e)
	658 (e)	681	726	771	709	795
	356 (e)	190 (e)	286 (e)	276 (e)	250 (e)	160 (e)
	734*i*	1194*i*	848*i*	−	1050*i*	1373*i*
energy						
$\Delta E^{\ddagger}$	9.4	9.3[g]	8.9	10.7	10.7	9.7
$\Delta H^{\ddagger}$ (0 K)	8.8	8.9		10.8	10.4	9.6
			H−Channel			
r_{C-Cl}	1.742	1.750	1.738	1.750	1.747	1.737
r_{C-H}	1.086	1.085	1.087	1.079	1.078	1.086
r_{C-Hr}	1.307	1.345	1.364	1.367	1.344	1.370
r_{Hb-Hr}	0.946	0.924	0.893	0.893	0.923	0.893
$\angle_{Cl-C-Hr}$	103.4	108.7	108.6	108.1	111.8	108.3
$\angle_{H-C-Hr}$	103.6	104.3	103.9	103.9	104.5	108.5
$\angle_{Hb-H-C}$	180.0	180.0	180.0	178.2	178.7	178.6
frequency	3264	3283	3139	3285	3310	3272
	3243	3175	3029	3169	3200	3158
	1554	1602	1671	1781	1644	1800
	1489	1480	1411	1452	1476	1466
	1423	1283	1148	1216	1270	1219
	1332	1272	1134	1210	1253	1206
	1012	1073	1028	1052	1076	1080
	977	1055	1005	1012	1049	1029
	703	798	777	785	791	821
	603	553	506	532	553	552
	343	313	287	295	318	315
	1193*i*	1794*i*	1277*i*		1590*i*	1803*i*
energy						
$\Delta E^{\ddagger}$	11.8	12.6[g]	10.9	13.4	12.8	12.5
$\Delta H^{\ddagger}$ (0 K)	10.9	10.8		11.8	11.1	11.2

[a] Distances in angstrom, angles in degrees, and energies in kcal mol^{-1}. [b] CCSD(T)/6-31G(d,p). This work. [c] UMP2/6-31G(d,p).[14] [d] UMP2/6-311G(2d,2p).[15] [e] BH&H-LYP/6−311 g(d,p).[16] [f] UMP2/6-311++G(d,p).[17] [g] Extrapolated IB energies. This work.

for each channel (i.e., the branching ratios) are not experimentally available, and only the overall rate constant is known. Therefore, in this paper, the rate constants were not used in the calibration.

3. Tests of Consistency of the Calibration. The results of the final fit for each channel are listed in Table 2 for reactants and products and in Table 3 for the saddle point. In general, the reactant and product properties agree with the experimental data,[22] with enthalpies of reaction at 0 K of −18.3 and −4.4 kcal mol^{-1}, vs the experimental value of −19.9 and −5.2 kcal mol^{-1} for the Cl- and H-abstraction channels, respectively. This agreement is, obviously, a consequence of the fitting procedure used, and it represents simply a check of the consistency of the parametrization. Both channels are exothermic, and since the chlorine abstraction channel is more exothermic by about 15 kcal mol^{-1}, a priori, based on thermochemical reasoning, one can expect that it will be the most favorable pathway. Clearly, the difference in exothermicity between the two channels is due to the bond dissociation energies (BDE's), larger for the C−H bond (100.1 ± 0.6 kcal mol^{-1})[23] than for the C−Cl bond (83.7 ± 0.4 kcal mol^{-1}).[24]

With respect to the CH_2Cl free radical, the experimental results[25,26] stablish that the structure deviates only slightly from planarity (C_s symmetry), while previous ab initio calculations[27,28] found a planar structure (C_{2v} symmetry). We have performed

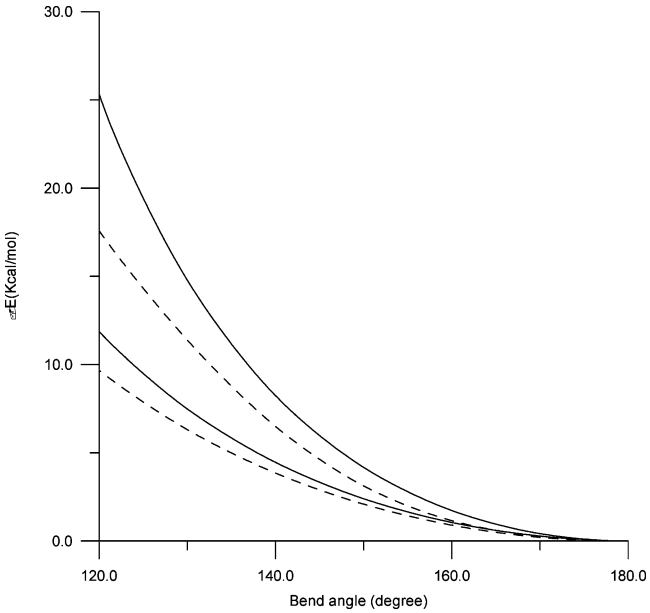

Figure 1. Saddle point bending-energy curves (C−Cl−H and C−H−H) for the CH_3Cl + H reaction on the two channels: Chlorine (two upper curves) and hydrogen (two lower curves) abstractions. PES results (full line) and ab initio MP2/6-31G(d,p) calculation (dashed line). The remaining internal coordinates were kept fixed for the respective methods. Note that the value of 180° corresponds to the saddle point.

ab initio calculations for this radical at three levels, MP2=FULL/6-31G(d,p); CCSD(T)/6-31G(d,p), and MP2=FULL/cc-pVTZ (Table 2). The two first levels, using the smallest basis set, yield a nonplanar structure, while the planar structure is not a true minimum (characterized by one imaginary frequency). When the largest basis set is used (cc-pVTZ) both planar (C_{2v} symmetry) and nonplanar (C_s symmetry) conformations were found and characterized. In all three levels the energy difference between both structures is practically negligible (<0.01 kcal mol^{-1}). In the present context, this implies that there are practically no differences in using either the planar or the nonplanar conformations for the theoretical study. With our PES we obtain that the CH_2Cl free radical is planar, although the values of 120° for the H−C−H and Cl−C−H angles represent excessive tightness for this compound.

With respect to the saddle point geometries, in general they reproduce well the ab initio information, with the most significant differences being for the Cl−Hb distance of the Cl-channel, which is larger than the ab initio data, and for the Cl−C−Hr angle of the H-channel which is 5° smaller than ab initio calculations.

Each saddle point was identified by having one negative eigenvalue of the Hessian matrix, and therefore one imaginary frequency, and their properties show reasonable agreement with the sparse ab initio and DFT quantum chemical calculations. The absolute values of the imaginary part of these frequencies are lower in our calculations than the ab initio values, although it is well-known that sometimes ab initio calculations overestimate this value.[29] This means that the saddle-point region is narrower in the PES than it should be, and that the tunneling factors could be overestimated at low temperatures. These two questions will be considered in sections III.4 and IV.1, respectively.

Both transition states are "early", i.e., they are reactant-like transition states, where the length of the bond that is broken increases by only 11% (C−Cl) and 6% (C−H) for the chlorine and hydrogen abstraction channels, respectively. For each

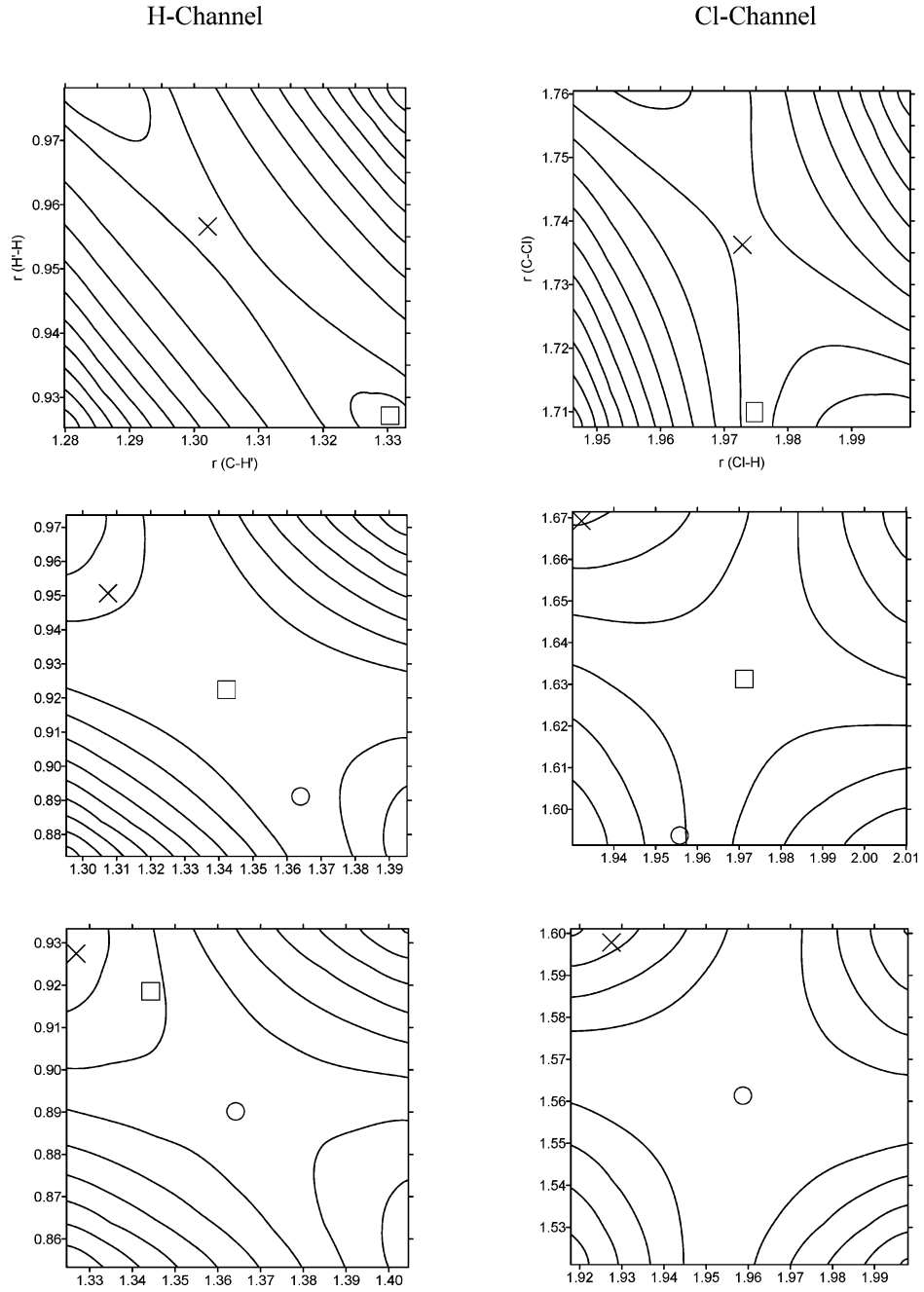

Figure 2. Contour plots of the saddle point zone for the chlorine (right panels) and hydrogen (left panels) abstraction channels using our analytical PES (first panel), CCSD(T)/6-31G(d,p) ab initio level (intermediate panel) and MP2/6-31G(d,p) ab initio level (third panel). The contours are shown for 0.1 kcal mol^{-1} increments with the maximum value at the saddle point. The symbols ×, □, and ○ mean the respective saddle points at the PES, CCSD(T) and MP2 levels. When in a panel a symbol does not appear, this means that it is outside the represented range of distances. The axis labels are the same for the three plots.

channel, the combined effect of potential energy and zero-point energy, i.e., $\Delta H_o^{\ddagger}$, the conventional transition-state enthalpy of activation at 0 K, is in good agreement with the values predicted by ab initio calculations (Table 3).

4. Test of Consistency of the New PES. Comparison with ab Initio Calculations. To confirm the accuracy and behavior of our analytical PESs, we calculated a grid of configurations using ab initio calculations in sensitive zones of the reaction, such as the bending of the linear approach, and the saddle point zone. As the objective is the simple comparison of the tendency, we used only ab initio calculations of a modest level.

With respect to the first point, it is well-known that there is a reasonable correlation between the bending frequency of the collinear saddle point (C−Y−A angle for the A + $CX_3Y \rightarrow$ AY + CX_3 reaction, and C−X−A angle for the A + $CX_3Y \rightarrow$ AX + CX_2Y reaction) and the product AY or AX rotational distributions. Schatz et al.[30,31] found that surfaces with the same saddle point but different dependence of the energy on the bending angle showed very different rotational excitation in the AY or AX product, concluding that looser saddle points imply hotter rotations. To test this energy dependence, we carried out ab initio calculations of the bending-energy curves (C−Cl−H and C−H−H angles for the chlorine and hydrogen abstraction channels, respectively), comparing them with the values from our analytical PES (Figure 1). Near the saddle point (bend angle of 180°) the analytical PES and the ab initio MP2/6-31G(d,p) curves show qualitative agreement for both channels, in general the PES energies being more repulsive than the ab initio ones.

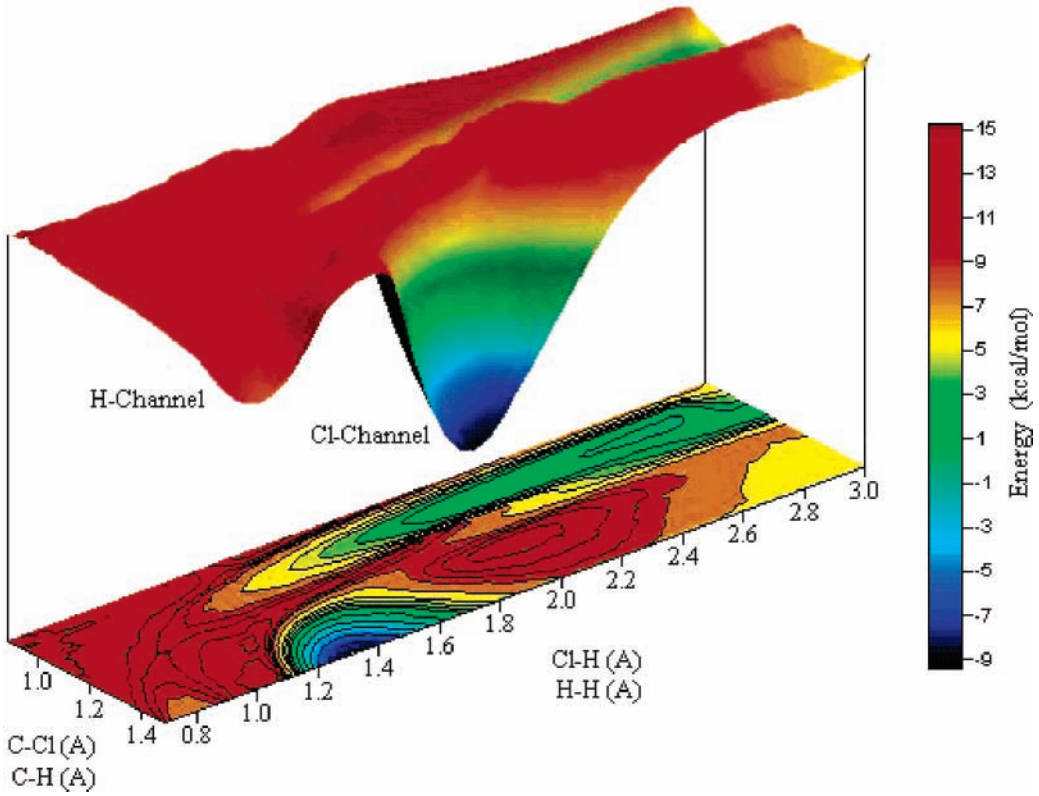

Figure 3. Potential energy surface and contour plots for the gas-phase $CH_3Cl + H \rightarrow$ Products reaction, where the two channels (chlorine and hydrogen abstraction) are included. For the Cl-channel the axes represent C−Cl against Cl−H, while for the H-channel they are C−H against H−H. All distances are given in angstroms.

This similar behavior of the two methods with respect to the bending mode would lead to similar ClH or H_2, respectively, rotational excitations. Note that Figure 1 represents a very wide range of values, from 180 to 120°, which is highly improbable in thermal experimental conditions. However, this wide range is very interesting theoretically to emphasize the behavior of the analytical PES with respect to a modest ab initio calculation. Clearly, other ab initio calculations of higher level were not considered.

With respect to the second point, Figure 2 shows contour plots in the neighborhood of the saddle point using our analytical PES and ab initio calculations [MP2/6-31G(d,p) and CCSD-(T)/6-31G(d,p)] for the two channels independently. First, for each channel, we observe that the location of the saddle point is strongly dependent on the level used, with the expensive CCSD(T) ab initio level intermediate between the analytical PES and the less costly MP2 ab initio level. This indicates that ab initio calculations with highly correlated wave functions and large basis sets are necessary for a correct description of the reaction, which, together with the large number of configuration needed for a complete description of the global surface, makes the description of polyatomic systems ($N > 4$ atoms) still today prohibitive (or at least highly expensive). Second, the three contour plots for each channel show qualitative agreement, describing in a similar way the reaction valley. For both channels, the analytical PES presents a narrower valley than the ab initio calculations.

In sum, the agreement achieved between the ab initio calculations and the description of the new PES in sensitive zones of the reactive system serves as additional confirmation of the accuracy of the new PES.

5. Applications and Advantages. The final functional form of the new PES and the adjustable parameters for each channel are given on our web page,[32] and a three-dimensional representation and the contour plots are shown in Figure 3. What is the applicability of this surface? First, it is applicable to any polyatomic system of the type $A + CX_3Y \rightarrow$ products. This permits one to study rapidly and accurately the influence of a new substituent (Y) and/or a new abstractor atom (A) on the kinetics and dynamics of the reaction. For instance, one could replace the Cl atom by F, Br or I.

Second, it permits one to study the branching ratios between two channels using the same functional form and calibrating each channel independently.

Third, it extends the field of application of the recent new hybrid method developed in our laboratory[33] to study large reactive systems. This hybrid approach is based on integrated methods where calculations for a small model system are performed by using analytical energy surfaces (AF), and for the real system by using molecular orbital (QM) or molecular mechanics (MM) methods. This hybrid method was denoted AF/QM or AF/MM, depending on the low level used to describe the real system.

Fourth, it can be used for trajectory calculations. These four applications represent a clear advantage, because there is a considerable saving in computation time with respect to other alternatives of constructing potential energy surfaces in polyatomic reactions.

6. Dynamical Calculations. With the new surface calibrated as described in the previous section for each channel independently, the reaction path was calculated starting from the respective saddle point geometry and going downhill to both reactants and products in mass-weighted Cartesian coordinates, using Page and McIver's method[34] with a step-size of 0.001 amu$^{1/2}$ bohr. The Hessian matrix was evaluated at every point along this reaction path. Along this minimum energy path (MEP), the reaction coordinate, s, is defined as the signed distance from the saddle point, with $s > 0$ referring to the

product side. In the rest of paper, the units of s are bohr, and all calculations are carried out in mass-scaled coordinates with a reduced mass μ equal to 1 amu. Thus, distances through the mass-scaled coordinates in bohr are equivalent to distances through mass-weighted coordinates in amu$^{1/2}$ bohr. We calculated the reaction path between $s = -2.0$ bohr and $s = +2.0$ bohr.

Along the MEP a generalized normal-mode analysis was performed using a curvilinear projection operator[35] formalism. With this information, we calculated, first, the ground-state vibrationally adiabatic potential curve

$$V_a^G(s) = V_{MEP}(s) + \epsilon_{int}^G(s) \quad (11)$$

where $V_{MEP}(s)$ is the classical energy along the MEP with its zero energy at the reactants ($s = -\infty$), and $\epsilon_{int}^G(s)$ is the zero-point energy at s from the generalized normal-mode vibrations orthogonal to the reaction coordinate; and second, the coupling terms,[36] $B_{k,F}(s)$, measuring the coupling between the normal mode k and the motion along the reaction coordinate, mode F. These coupling terms are the components of the reaction path curvature, $\kappa(s)$, defined as

$$\kappa(s) = \left(\sum [B_{k,F}(s)]^2\right)^{1/2} \quad (12)$$

and they control the nonadiabatic flow of energy between these modes and the reaction coordinate.[37,38] These coupling terms will allow us to calculate accurate semiclassical tunneling factors, and to give a qualitative explanation of the possible vibrational excitation of reactants and/or products, i.e., dynamical features, which are another sensitive test of the new surface.

Figure 4 shows the classical potential energy, V_{MEP}, and the ground-state vibrationally adiabatic potential energy relative to reactants, $\Delta V_a^G(s)$, as functions of s over the range $s = -2.0$ to $s = +2.0$ bohr, for the Cl- and H-channels.

On the basis of the information for each channel independently, rate constants were estimated by using improved canonical variational transition-state theory (ICVT).[39,40] Quantum effects on motions transversal to the reaction-path were included by using quantum-mechanical vibrational partition functions under the harmonic oscillator approach, while quantum effects in the motion along the reaction-path were included by using the microcanonical optimized multidimensional tunneling (μOMT) method, in which (at each energy) the transmission probability is taken as the maximum of two trial calculations, namely, small-curvature tunneling (SCT)[41] and large-curvature tunneling (LCT)[42] methods. All dynamical calculations were performed using the general polyatomic rate constants code POLYRATE.[43] The rotational partition functions were calculated classically, and the vibrational modes were treated as quantum mechanical separable harmonic oscillators.

IV. Results and Discussion

1. Rate Constants and Branching Ratio. With this PES, we calculated the rate constants for each channel independently, which permits us to calculate the branching ratio, an experimentally unknown measurement. Rate constants were estimated by using improved canonical variational transition-state theory (ICVT) with the microcanonical optimized multidimensional tunneling method (μOMT), in short, ICVT/μOMT, and the results are given in Table 4. These results show that the Cl-abstraction reaction (R1) is the predominant channel until 2100 K, while above this temperature the H-abstraction is favored. In the common temperature range used by several theoretical studies, these results agree with those found by Bryukov et al.[14] and Louis et al.,[17] but disagree with those found by Knyazev[15] and Sheng et al.[16] Note that none of these theoretical studies noted the change of channel with temperature predicted in the present work.

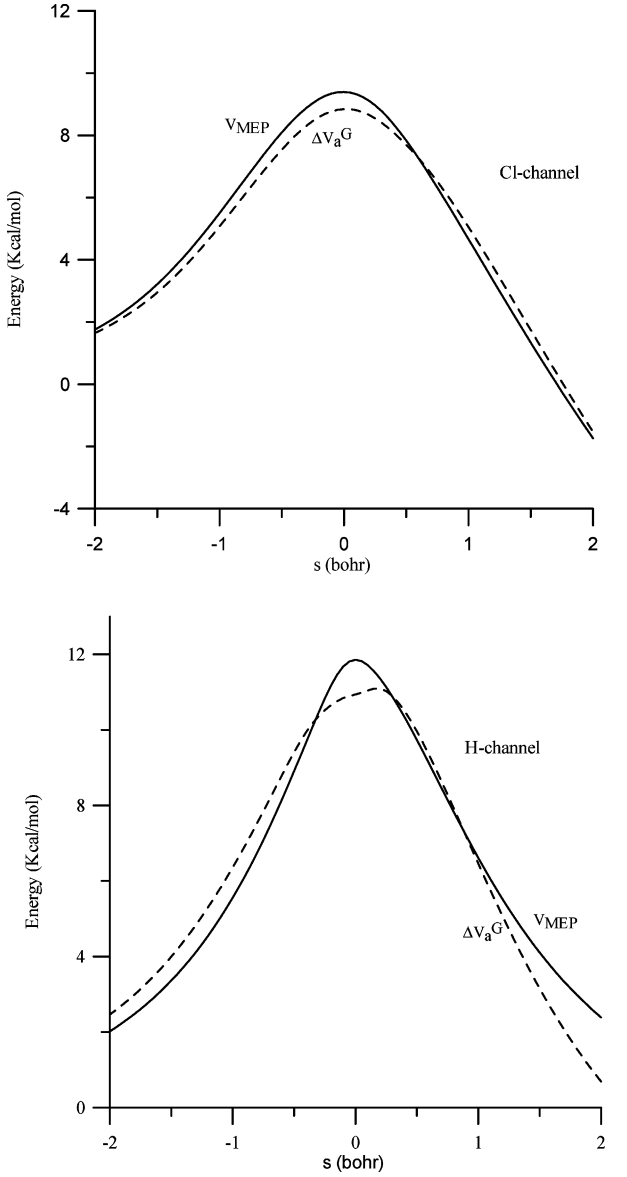

Figure 4. Classical potential energy curve, V_{MEP}, and vibrationally adiabatic potential energy curve, ΔV_a^G, as a function of reaction coordinate s, for the Cl- and H-channels. All quantities are with respect to the reactants.

To understand this behavior, we analyzed the evolution of the enthalpy and entropy changes as a function of temperature for both channels. The free energy of activation, $\Delta G°(T,s)$, determines the thermal rate constant, and can be thermochemically written as a sum of enthalpy and entropy contributions

$$\Delta G°(T,s) = \Delta H°(T,s) - T\Delta S°(T,s) \quad (13)$$

When the reaction evolves from reactants to the transition state, $\Delta S°(T,s)$ becomes more negative, and the term $-T\Delta S°(T,s)$ becomes more positive, increasing with temperaure. The Cl-channel presents a lower enthalpy change than the H-channel over all the temperature range, 298−3000 K, being therefore the favored pathway by enthalpy reasons. For instance, at 0 K, where the term $-T\Delta S°(T,s)$ vanishes, the adiabatic barrier

TABLE 4: Rate Constants (cm^3 molecule^{-1} s^{-1}) for Both Channels and Branching Ratios

	Cl-channel			H-channel			ratio (Cl)[d]		
T (K)	ICVT/μOMT[a]	SLLXS[b]	LGS[c]	ICVT/μOMT	SLXS	LGS	PES	SLXS	LGS
298	7.96E−18	1.54E−18		1.43E−18	1.54E−19	-	0.848	0.909	
300	8.75E−18		8.43E−18	1.59E−18		1.44E−18	0.847		0.854
350	6.80E−17		8.13E−17	1.54E−17		1.73E−17	0.815		0.825
400	3.33E−16	8.68E−17	4.58E−16	9.11E−17	3.24E−16	1.13E−16	0.785	0.211	0.802
500	3.38E−15	1.18E−15	5.49E−15	1.22E−15	3.13E−15	1.63E−15	0.735	0.274	0.771
600	1.71E−14		3.07E−14	7.44E−15		1.02E−14	0.696		0.751
700	5.71E−14		1.10E−13	2.86E−14		3.93E−14	0.666		0.737
800	1.46E−13		2.98E−13	8.17E−14		1.13E−13	0.642		0.725
900	3.12E−13	1.28E−13	6.63E−13	1.90E−13	2.79E−13	2.63E−13	0.622	0.314	0.716
1000	5.84E−13	2.49E−13	1.28E−12	3.83E−13		5.31E−13	0.604		0.707
1500	4.43E−12		1.10E−11	3.72E−12		5.32E−12	0.543		0.674
2000	1.39E−11	6.54E−12	3.70E−11	1.36E−11	2.03E−11	2.00E−11	0.505	0.244	0.649
2100	1.65E−11		4.46E−11	1.66E−11		2.46E−11	0.498		0.645
2200	1.93E−11		5.30E−11	1.99E−11		2.97E−11	0.492		0.641
2300	2.25E−11		6.23E−11	2.37E−11		3.54E−11	0.487		0.638
2400	2.58E−11		7.24E−11	2.78E−11		4.18E−11	0.481		0.634
2500	2.94E−11		8.33E−11	3.23E−11		4.88E−11	0.476		0.631
2600	3.32E−11			3.72E−11			0.471		
2700	3.72E−11			4.26E−11			0.467		
2800	4.15E−11			4.83E−11			0.462		
2900	4.60E−11			5.44E−11			0.458		
3000	5.07E−11	2.40E−11		6.09E−11	9.55E−11		0.454	0.201	

[a] This work. [b] Reference 16. [c] Reference 17. [d] τ (Cl) = k(Cl)/[k(Cl) + k(H)]. Obviously, the ratio for the H-channel is simply its complement.

TABLE 5: Transmission Coefficients (κ) for Both Channels

	Cl-channel					H-channel				
	PES					PES				
T(K)	Wigner	SCT	μOMT	SLLXS SCT[a]	LGS Wigner[b]	Wigner	SCT	μOMT	SLLXSSCT[a]	LGS Wigner[b]
298	1.5	1.7	1.7	4.4		2.4	4.2	4.2	45.7	
300	1.5	1.7	1.7		2.8	2.4	4.1	4.2		4.1
350	1.4	1.5	1.5		2.3	2.0	2.8	2.8		3.3
400	1.3	1.3	1.3	2.1	2.0	1.8	2.2	2.2	7.0	2.8
500	1.2	1.2	1.2	1.6	1.7	1.5	1.6	1.6	3.2	2.1
600	1.1	1.1	1.1		1.5	1.3	1.4	1.4		1.8
700	1.1	1.1	1.1		1.3	1.3	1.3	1.3		1.6
800	1.1	1.1	1.1		1.3	1.2	1.2	1.2		1.4
900	1.1	1.1	1.1	1.1	1.2	1.2	1.2	1.2	1.4	1.4
1000	1.0	1.0	1.0	1.1	1.2	1.1	1.1	1.1	1.3	1.3
1500	1.0	1.0	1.0		1.1	1.1	1.1	1.1		1.1
2000	1.0	1.0	1.0	1.0	1.0	1.0	1.0	1.0	1.1	1.1
2100	1.0	1.0	1.0		1.0	1.0	1.0	1.0		1.1
2200	1.0	1.0	1.0		1.0	1.0	1.0	1.0		1.1
2300	1.0	1.0	1.0		1.0	1.0	1.0	1.0		1.1
2400	1.0	1.0	1.0		1.0	1.0	1.0	1.0		1.1
2500	1.0	1.0	1.0		1.0	1.0	1.0	1.0		1.0
2600	1.0	1.0	1.0			1.0	1.0	1.0		
2700	1.0	1.0	1.0			1.0	1.0	1.0		
2800	1.0	1.0	1.0			1.0	1.0	1.0		
2900	1.0	1.0	1.0			1.0	1.0	1.0		
3000	1.0	1.0	1.0	1.0		1.0	1.0	1.0	1.0	

[a] Reference 16. [b] Reference 17.

heights, $\Delta H°(0K,s) = \Delta V_a^G(s) = \Delta G°(0K,s)$, are 8.8 and 10.9 kcal mol^{-1} for the Cl- and H-channels, respectively (Table 3). However, the entropy change $[-T\Delta S°(T,s)]$ always favors the H-channel. At $T < 2100$ K, the difference of $\Delta H°(T,s)$ between the two channels is larger than the difference of $[-T\Delta S°(T,s)]$, favoring the Cl-channel: $\Delta[\Delta H°(T,s)] > \Delta[-T\Delta S°(T,s)]$. However, at $T > 2100$ K, the order is inverted: $\Delta[\Delta H°(T,s)] < \Delta[-T\Delta S°(T,s)]$, favoring, therefore, the H-channel. At $T = 2100$ K, one has the situation where the two terms are compensated.

With respect to the tunneling effect (Table 5), the transmission coefficient, which mostly takes into account quantum effects in the motion along the reaction-path, increases the rate constants by small factors, 1.7−1.0, and by larger factors, 4.2−1.0, for the Cl- and H-channels, respectively, over the temperature range 298−3000 K. This behavior was to be expected, since the Cl-channel involves the motion of a heavy particle (a chlorine atom) that cannot easily tunnel through the reaction barrier, while the H-channel represents the typical situation of a good candidate for a large tunneling effect. Louis et al.[17] using the very modest Wigner method to describe the tunneling found similar values for the H-channel, but larger values for the Cl-channel. Given that this last reaction involves the motion of a heavy particle, our results seem physically more reasonable.

It is interesting to note that, because the values of the tunneling factors for both channels are small, and the studied temperature range, 298−3000 K, does not include very low temperatures, the effect of the underestimation of the imaginary

TABLE 6: Total Rate Constants (cm^3 molecule^{-1} s^{-1}) for the $CH_3Cl + H \rightarrow$ Products Reaction

		expt		theor		
T (K)	PES	WdH[a]	BSK[b]	K[c]	SLLXS[d]	LGS[e]
298	9.39E−18					
300	1.03E−17			2.85E−17	1.57E−17	9.87E−18
350	8.35E−17			1.52E−16		9.86E−17
400	4.24E−16			6.75E−16		5.71E−16
500	4.59E−15	5.29E−15		5.54E−15	4.31E−15	7.12E−15
600	2.45E−14	2.52E−14	2.79E−14	2.64E−14		4.09E−14
700	8.57E−14	7.67E−14	1.01E−13	8.51E−14		1.49E−13
800	2.28E−13	1.77E−13	2.64E−13	2.13E−13		4.10E−13
900	5.02E−13			4.50E−13	4.07E−13	9.26E−13
1000	9.66E−13			8.39E−13	8.03E−13	1.82E−12
1500	8.14E−12			6.62E−12		1.63E−11
2000	2.74E−11			2.25E−11	2.68E−11	5.70E−11
2100	3.31E−11					
2200	3.93E−11					
2300	4.61E−11					
2400	5.36E−11				5.47E−11	
2500	6.17E−11			5.23E−11		1.32E−10
2600	7.05E−11					
2700	7.98E−11					
2800	8.98E−11					
2900	1.00E−10					
3000	1.12E−10					

[a] Values from the expression $k(T) = 6.14 \times 10^{-11} \exp(-9300/RT)$ cm^3 molecule^{-1} s^{-1}; 500−800 K.[10] [b] Values from the expression: $k(T) = (2.24 \pm 0.75) \times 10^{-10} \exp(-5394 \pm 202\ \mathrm{K}/T)$ cm^3 molecule^{-1} s^{-1}; 586−839 K.[14] [c] Reference 15. [d] Reference 16. [e] Reference 17.

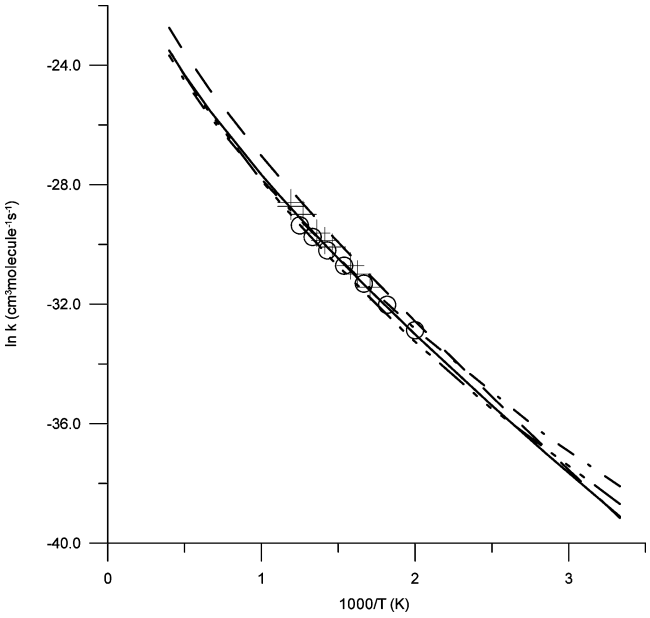

Figure 5. Arrhenius plot of ln k (cm^3 molecule^{-1} s^{-1}) for the overall reaction against the reciprocal of the temperature (K) in the range 298−3000 K for the forward thermal reaction. (○) Exp. values from ref 10. (×) Experimental values from ref 14. Full line: Theoretical values from this work. Dashed−dotted line: Theoretical values from ref 15. Dashed-triple-dotted line: Theoretical values from ref 16. Dashed line: Theoretical values from ref 17.

frequencies at the saddle point mentioned in section III.3 is not so important in this case.

The overall rate constants are obtained from the sum of the values for each channel and are given in Table 6, together with the experimental and other theoretical values for comparison, and Figure 5 shows the corresponding Arrhenius plot. Our results show excellent agreement with the experimental information in the common temperature range, 500−800 K, and, given that these values were not used in the calibration process, this lends confidence to the new potential energy surfaces. While

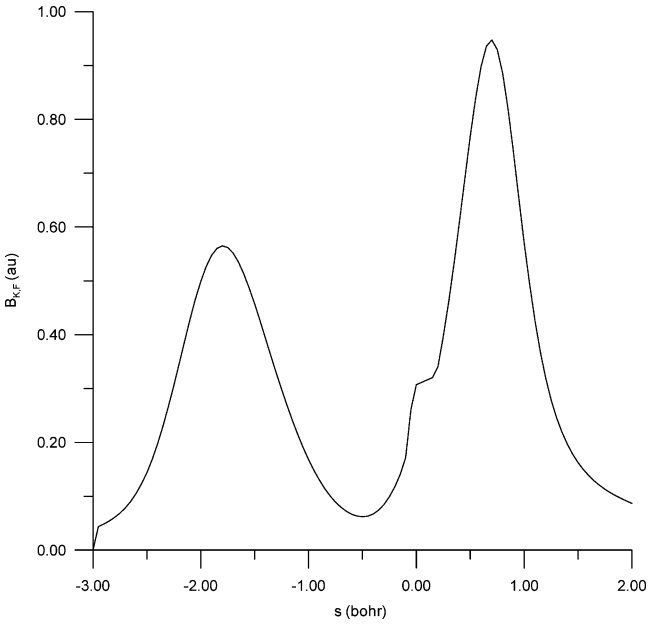

Figure 6. Chlorine channel. Curvature elements, $B_{k,F}(s)$. Coupling along the MEP between the reaction coordinate (F) and the reactive mode.

the theoretical results of Sheng et al.[16] underestimate the experimental rate constants by factors of 0.81−0.71 in the common range, 500−800 K, the agreement found by Knyazev[15] using a modest TST-Eckart based model is only a consequence of the fitting procedure used by that author to reproduce the experimental information.

All the rate constants calculated in this work show a small curvature of the Arrhenius plots, and we fit our results to a three-term expression of the type $k(T) = AT^n \exp(-B/T)$. The resulting equations in units of cm^3 molecule^{-1} s^{-1} are

$$k(R_1) = 7.281 \times 10^{-17} \mathrm{T}^{1.8496} \exp(-3812.3/T), \quad \text{Cl-channel}$$

$$k(R_2) = 2.576 \times 10^{-18} T^{2.3058} \exp(-4097.1/T), \quad \text{H-channel}$$

$$\mathrm{k(total)} = 1.403 \times 10^{-17} T^{2.1536} \exp(-3787.6/T), \quad \text{overall reaction}$$

2. Curvature Terms, $B_{k,F}(s)$. Another important feature of the new PES is the description of the possible vibrational excitation in the entry and exit channels. The coupling terms $B_{k,F}(s)$ between the reaction coordinate and the orthogonal bound modes control the nonadiabatic flow of energy between these modes. Figures 6 and 7 show these coupling terms as a function of s for the Cl- and H-abstraction channels, respectively. We begin by analyzing the Cl-channel (Figure 6). There are two peaks, one on the reactant side and one on the product side. The first is due to the strong coupling of the reaction coordinate to the C−Cl reactive stretch of halomethane, and appears at $s = -1.8$ bohr. Therefore, a priori, excitation of this mode might be expected to enhance the reaction rate. The second peak is in the exit channel ($s = +0.6$ bohr), and it is due to the coupling of the reaction path to the Cl−H stretch. This indicates that this product mode could appear vibrationally excited. With respect to the H-channel (Figure 7), we also found two peaks. The first is in the entry channel ($s = -0.35$ bohr) and is due to the coupling of the reaction coordinate to the C−H reactive stretching mode, indicating, a priori, that excitation of this mode could enhance the rate. The second peak is in the exit channel ($s = +0.10$ bohr), and is due to the coupling of the reaction

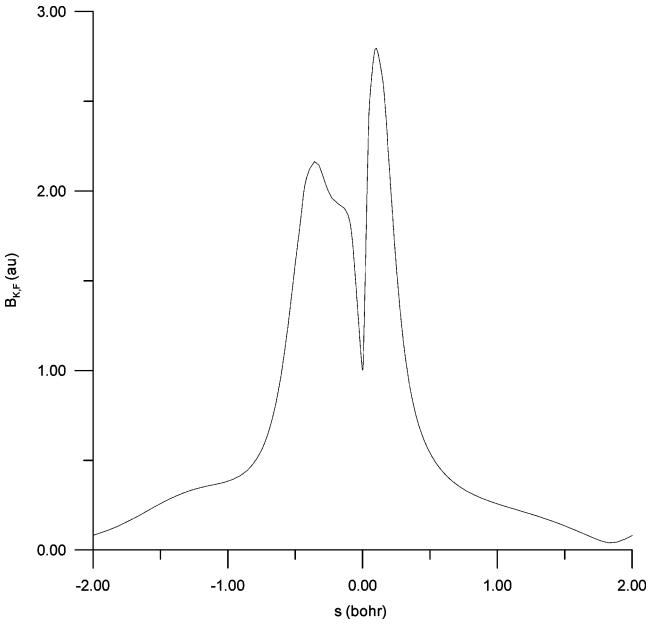

Figure 7. Hydrogen channel. Curvature elements, $B_{k,F}(s)$. Coupling along the MEP between the reaction coordinate (F) and the reactive mode.

path to the H−H stretch, indicating, a priori, that this product mode could appear vibrationally excited. This dynamic analysis is consistent with "early" transition states (as were obtained with the present analytical PESs) where the products are formed with vibrational excitation.[33,44−46] Unfortunately, to the best of our knowledge, there is no experimental information for comparison. These questions therefore represent an exciting experimental challenge in their detailed verification.

V. Conclusions

In this work we have carefully investigated the gas-phase $CH_3Cl + H \rightarrow CH_3 + ClH$ (R1) and $CH_2Cl + H-H$ (R2) reactions, which proceed by two channels, Cl- and H-abstraction, as a model of a more general asymmetrically substituted polyatomic system, $CX_3Y + A$. We constructed the analytical potential energy surface for each channel independently, using the same functional form and two different sets of parameters. As calibration criteria we used only the stationary point properties (geometry, vibrational frequencies, and energy changes). The new surfaces are attractive, i.e., both channels have an "early" transition state (reactant-like transition-state).

For the Cl- and H-channels independently, and for the overall reaction (from the sum of the individual rate constants) the forward thermal rate constants were calculated over a wide temperature range, 298−3000 K, using the variational ICVT/μOMT method with curvilinear coordinates. The calculated rate constants for the two channels and the overall reaction show small curvatures of the Arrhenius plots, indicating the role of the tunneling factor, mainly due to the H-abstraction channel. For the total reaction, to which corresponds the only experimental information available, our theoretical results agree with experiment in the common temperature range, 500−800 K. This result is encouraging because, first, this experimental information was not used in the parameter fitting and, second, it was obtained from the sum of two individual rate constants. This kinetics result lends support to the PESs constructed in this work.

The analysis of the reaction-path curvature qualitatively showed that, for the Cl-channel, excitation of the C−Cl stretch reactive mode might be expected to enhance the rate constants and that the Cl−H stretch mode in the product can appear vibrationally excited; while for the H-channel, the modes involved are the C−H stretch reactive mode in the reactants, and the H−H stretch in the products.

Finally, the agreement between our theoretical results and the available experimental measurements (geometry, energy, and kinetics) lends confidence to the newly constructed PESs, which can be used for trajectory calculations to study, in an economical way, the effects of the substituents.

Acknowledgment. We are grateful to Prof. Donald G. Truhlar for providing a copy of the POLYRATE program, to Dr José C. Corchado for computational support, and to the Consejeria de Educación, Ciencia y Tecnología, Junta de Extremadura (Spain) (Project No. 2PR04A001) for partial financial support of this work

References and Notes

(1) Espinosa-García, J. *J. Chem. Phys.* **1999**, *111*, 9330.
(2) Espinosa-García, J.; García-Bernáldez, J. C *Phys. Chem. Chem. Phys.* **2000**, *2*, 2345.
(3) Corchado, J. C.; Truhlar, D. G.; Espinosa-García, J. *J. Chem. Phys.* **2000**, *112*, 9375.
(4) Espinosa-García, J.; Corchado, J. C. *J. Chem. Phys.* **2000**, *112*, 5731.
(5) Espinosa-García, J. *J. Chem. Phys.* **2002**, *116*, 10664.
(6) Espinosa-García, J. *J. Chem. Phys.* **2002**, *117*, 2076.
(7) Rangel, C.; Navarrete, M.; Espinosa-García, J. *J. Phys. Chem. A* **2005**, *109*, 1441.
(8) Rangel, C.; Espinosa-García, J. *J. Chem. Phys.* **2005**, *122*, 134315.
(9) Hart, L. W.; Grunfelder, C.; Fristrom, R. M. *Combust. Flame* **1974**, *23*, 109.
(10) Westenberg, A. A.; deHass, N. J. *J. Chem. Phys.* **1975**, *62*, 3321.
(11) Aders, W. K.; Pangritz, D.; Wagner, H. Gg. *Ber. Bunsen-Ges. Phys. Chem.* **1975**, *79*, 90.
(12) Jones, W. E.; Ma, J. L. *Can. J. Chem.* **1986**, *64*, 2192.
(13) Triebert, J.; Meinike, T.; Olzmann, M.; Scherzer, K. *Z. Phys. Chem. (Munich)* **1995**, *191*, 47.
(14) Bryukov, M. G.; Slagle, I. R.; Knyazev, V. D. *J. Phys. Chem. A* **2001**, *105*, 3107.
(15) Knyazev, V. D. *J. Phys. Chem. A* **2002**, *106*, 11603.
(16) Sheng, L.; Li, Z. S.; Liu, J. Y.; Xiao, J. F.; Sun, Ch. Ch. *J. Chem. Phys.* **2003**, *118*, 4920.
(17) Louis, F.; Gonzalez, C.; Sawerysyn, J. P. *J. Phys. Chem. A* **2004**, *108*, 10586.
(18) Truhlar, D. G. *Chem. Phys. Lett.* **1998**, *294*, 45.
(19) Fast, P. L.; Sánchez, M. L.; Truhlar, D. G. *J. Chem. Phys.* **1999**, *111*, 2921.
(20) Kendall, R. A.; Dunning, T. H.; Harrison, R. J. *J. Chem. Phys.* **1992**, *96*, 6796.
(21) Duchovic, R. J.; Hase, W. L.; Schlegel, H. B. *J. Phys. Chem.* **1984**, *88*, 1339.
(22) Chase, M. W.; Davis, C. A.; Downey, J. R.; Frurip, D. J.; McDonald, R. A.; Syverud, A. N. JANAF Thermochemical tables. *J. Phys. Chem. Ref. Data Suppl.* **1985** 14.
(23) Seetula, J. A. *J. Chem. Soc., Faraday Trans.* **1996**, *92*, 3069.
(24) Pedley, J. B.; Naylor, R. D.; Kirby, S. P. *Themochemcial Data of Organic Compounds*, 2nd ed.; Chapman and Hall: New York, 1986.
(25) Endo, Y.; Saito, S.; Hirota, E. *Can. J. Phys.* **1984**, *62*, 1347.
(26) Sears, T. J.; Temps, F.; Wagner, H. G. G.; Wolf, M. *J. Mol. Spectrosc.* **1994**, *168*, 136.
(27) Li, Y.; Francisco, J. S. *J. Chem. Phys.* **2001**, *114*, 2879.
(28) Levchenko, S. V.; Krylov, A. I. *J. Chem. Phys.* **2001**, *115*, 7485.
(29) See e.g., Petersson, G. A.; Tensfeldt, T. G.; Montgomery, J. A. *J. Chem. Phys.* **1991**, *94*, 6091.
(30) Schatz, G. C.; Amaee, B.; Connor, J. N. L. *J. Chem. Phys.* **1990**, *92*, 4893.
(31) Troya, D.; Pascual, R. Z.; Schatz, G. C. *J. Phys. Chem. A* **2003**, *107*, 10497.
(32) http://w3qf.unex.es.
(33) Espinosa-García, J.; Rangel, C.; Navarrete, M.; Corchado, J. C. *J. Chem. Phys.* **2004**, *121*, 5098.
(34) Page, M.; McIver, J. W. *J. Chem. Phys.* **1988**, *88*, 922.
(35) Jackels, C. F.; Gu, Z.; Truhlar, D. G. *J. Chem. Phys.* **1995**, *102*, 3188.

(36) Miller, W. H.; Handy, N. C.; Adams, J. E. *J. Chem. Phys.* **1980**, *72*, 99.

(37) Morokuma, K.; Kato, S. In *Potential Energy Surfaces and Dynamics Calculations*; Truhlar, D. G., Ed.; Plenum: New York, 1981; p 243.

(38) Kraka, E.; Dunning, T. H. *Advances in Molecular Electronic Structure Theory*; JAI: New York, 1990; Vol. I, p 129.

(39) Garrett, B. C.; Truhlar, D. G.; Grev, R. S.; Magnuson, A. W. *J. Phys. Chem.* **1980**, *84*, 1730. Garrett, B. C.; Truhlar, D. G.; Grev, R. S.; Magnuson, A. W. *J. Phys. Chem.* **1983**, *87*, 4554(E).

(40) Truhlar, D. G.; Isaacson, A. D.; Garrett, B. C. In *The Theory of Chemical Reactions*; Baer, M., Ed.; Chemical Rubber: Boca Raton, FL, 1985; Vol. 4.

(41) Liu, Y.-P.; Lynch, G. C.; Truong, T. N.; Liu, D−h.; Truhlar, D. G. *J. Am. Chem. Soc.* **1993**, *115*, 2408.

(42) Truong, T. N.; Lu, D-h.; Lynch, G. C.; Liu, Y.-P.; Melissas, V. S.; Stewart, J. J.; Steckler, R.; Garrett, B. C.; Isaacson, A. D.; González-Lafont, A.; Rai, S. N.; Hancock, G. C.; Joseph, T.; Truhlar, D. G. *Comput. Phys. Commun.* **1993**, *75*, 43.

(43) Corchado, J. C.; Chuang, Y.-Y.; Fast, P. L.; Villa, J.; Hu, W.-P.; Liu, Y.-P.; Lynch, G. C.; Nguyen, K. A.; Jackels, C. F.; Melissas, V. S.; Lynch, B. J.; Rossi, I.; Coitiño, E. L.; Fernández-Ramos, A.; Steckler, R.; Garrett, B. C.; Isaacson, A. D.; Truhlar, D. G. POLYRATE, version 8.5.1, University of Minnesota, Minneapolis, MN, 2000.

(44) Polanyi, J. C.; Wang, W. H. *J. Chem. Phys.* **1969**, *51*, 1439.

(45) Perry, D. S.; Polanyi, J. C.; Wilson, C. W. *J. Chem. Phys.* **1974**, *53*, 317.

(46) Duff, J. W.; Truhlar, D. G. *J. Chem. Phys.* **1975**, *62*, 2477.